Journal of Cleaner Production 451 (2024) 142011

Contents lists available at ScienceDirect

Journal of Cleaner Production

journal homepage: www.elsevier.com/locate/jclepro

Development of sustainable engineered cementitious composite with enhanced compressive performance at elevated temperatures using high volume GGBFS

S. Rawat [a,b], Y.X. Zhang [a], D.J. Fanna [c], C.K. Lee [b,*]

[a] School of Engineering, Design and Built Environment, Western Sydney University, NSW, 2751, Australia
[b] School of Engineering and Technology, The University of New South Wales, Canberra, ACT, 2600, Australia
[c] Advanced Materials Characterisation Facility, Western Sydney University, NSW, 2116, Australia

ARTICLE INFO

Handling Editor: Jian Zuo

Keywords:
Elevated temperature
Engineered cementitious composite
Green construction material
Hybrid fibre
Residual compressive strength

ABSTRACT

This study presents the development of an environmentally sustainable hybrid polyethylene (PE)-steel fibre reinforced engineered cementitious composites (ECC) to achieve enhanced compressive performance at elevated temperature. Utilizing a unique blend of industry by-products—ground granulated blast furnace slag (GGBFS), dolomite powder, and fly ash, with supplementary cementitious materials exceeding 50% replacement level, the developed ECC achieves remarkable improvement in compressive strength, both at ambient and elevated temperature conditions. A total of 340-cylinder specimens were tested to analyse the compressive properties after exposure to 20–800 °C, and the effect of different binders, fibre ratio on the residual compressive behaviour was investigated. Additionally, effects of the critical fire test parameters such as pre-drying and cooling treatment were also studied. The research findings indicate that incorporating high-volume GGBFS blends significantly improved the compressive performance of the ECC irrespective of the type of test parameters. Notably, a specific blend comprising of GGBFS, fly ash (GGBFS:fly ash = 1:0.2) and dolomite (15% by binder weight) demonstrated 138 MPa strength at room temperature and at least 75% and 45% strength retention at 600 °C and 800 °C, respectively. This was significantly higher than the values reported in literatures (~48% at 600 °C and ~12% at 800 °C) for similar type of ECC. The study also highlights the impact of sudden cooling in water and confirms the occurrence of both thermal shock and rehydration through microstructural analysis. Environmental impact analysis was also conducted to demonstrate the low carbon emission of the developed ECC.

1. Introduction

Concrete is inherently fire resistant, and in most cases, normal concrete structures perform well under elevated temperatures without the need of any additional protection. With an increasing demand of improved forms of concrete, attempts have further been made to develop high performance fibre reinforced cementitious composites (FRCCs) such as strain hardening cementitious composite (SHCC), engineered cementitious composite (ECC) or ultra-high-performance concrete (UHPC) (Rawat et al., 2021). These composites exhibit pseudo strain-hardening behaviour due to the bridging action between the short fibres and matrix resulting in multiple fine cracks (Li, 2003) and have been successfully implemented in various construction projects due to their excellent mechanical properties and durability performance. However, dense microstructure and low permeability influence their fire performance adversely (Li et al., 2019a).

There has been significant research in recent years focused on improving the mechanical performance of FRCC at elevated temperatures (Rawat et al., 2021). However, the primary emphasis has been on the choice of fibre type or volume, and the effect of matrix constituents on residual performance has not been extensively investigated. In general, most of the studies take advantage of low melting point of polymer fibres such as polyvinyl alcohol (PVA) and polyethylene (PE) fibre and do not fully explore the potential of thermally better performing ***binder materials*** in improving the fire performance. This consideration is imperative given the substantial role of binder material at elevated temperature as evidenced from previous research on concrete. Existing literature have clearly highlighted the pronounced effect of the

* Corresponding author. School of Engineering and Technology, Room 133, Building 20, UNSW, Canberra, 2600, Australia.
E-mail address: chi.k.lee@unsw.edu.au (C.K. Lee).

https://doi.org/10.1016/j.jclepro.2024.142011
Received 29 January 2024; Received in revised form 10 March 2024; Accepted 27 March 2024
Available online 3 April 2024

industry-by products added as supplementary cementitious materials (SCM) at elevated temperatures (Magalhães et al., 2015; Phan and Carino, 2002; Sullivan and.Sharshar, 1992). For instance, fly ash (FA)-based concrete generally exhibits initial strength gain on exposure to elevated temperature due to the formation of tobermorite (Magalhães et al., 2015). On the other hand, presence of silica fume (SF) was found to negatively affect the residual compressive strength and elastic modulus of concrete due to high denseness of the microstructure (Phan and Carino, 2002). Explosive spalling has also been frequently associated with the use of silica fume due to the resulting high pore pressure and thermal gradient. Another type of SCM, ground granulated blast furnace slag (GGBFS) was found to demonstrate better performance than both fly ash and silica fume (Sullivan and Sharshar, 1992).

Despite the potential of different SCMs in improving the mechanical performance at elevated temperatures, majority of the studies on FRCC predominantly focus on using FA and SF in combination with a high proportion of cement (Rawat et al., 2021). Moreover, the studies on PE fibre reinforced ECC seem to have only considered SF as the primary SCM at a very low replacement ratio (Rawat et al., 2021). Consequently, the resulting composite not only carries significant environmental implications, but it also shows severe degradation (with more than 85% strength loss) at 800 °C due to the choice of the binder (Liu and Tan, 2018). This poor performance further poses a challenge in justifying the practical implementation of PE fibres in ECC. It is important to note that the inclusion of PE fibre is imperative for the development of environmentally friendly ECC with high mechanical performance. PE fibres not only have lower embodied energy per unit volume (Shoji et al., 2022), but also offer the potential for achieving both high compressive strength and ultimate tensile strain simultaneously (Ranade et al., 2013; Wu et al., 2021; Zhang et al., 2021a). Unlike commonly used PVA fibres, PE fibres also meet the criteria for developing ultra-high performance FRCC with high tensile strain capability (Liu and Tan, 2018). Therefore, to develop green ECC, it is crucial to analyse the role of alternative industry by-products which can not only bond well with PE fibre but may also have the potential to enhance ambient and elevated temperature performance.

In addition to the clear negligence towards consideration of the effect of matrix in assessing the fire performance, majority of these studies also tend to neglect the effect of the associated test parameters such as pre-drying treatment or type of cooling which could also affect the results significantly. A pre-drying or oven-drying procedure has commonly been used by many researchers to control explosive spalling (Rawat et al., 2021; Tang et al., 2023; Luo et al., 2022). This procedure usually involves heating specimens up to a certain temperature to allow the free moisture to escape which otherwise could hinder the testing process and may make it more prone to spalling. However, the commonly preferred pre-drying temperature range of 105 ± 5 °C may inadvertently impact the microstructure (Liang et al., 2018; Galle, 2001), and the exact impact of pre-drying on residual compressive strength remains doubtful. Furthermore, two types of cooling, namely air cooling and water cooling, have been used with the former being the most favoured. Water cooling is more realistic condition and is found to have both negative effect (due to thermal shock) and positive effect (due to rehydration) on the compressive strength with respect to the air cooling (Rawat et al., 2021). However, there is no clear consensus on its exact effect as well. Overall, the effect of different binder system together with these test parameters augments the overall complexity of the behavioural mechanism at elevated temperature, and therefore, it becomes important to understand the effect of each parameter such as binder material, type of cooling or pre-drying independently to gain further insight.

Therefore, this paper aims to develop green hybrid fibre reinforced ECC with enhanced residual compressive strength at elevated temperatures and conduct a comprehensive study on effect of matrix constituents and test parameters including pre-drying treatment and type of cooling. In the authors' previous work, a quaternary blend of GGBFS, fly ash and dolomite (with a total 60% cement replacement) was proposed to achieve optimized performance at ambient temperature (Rawat et al., 2022). Subsequently, various blends of same SCMs including GGBFS, fly ash and dolomite (keeping the total 60% cement replacement level) along with a standard mix with silica fume are considered to investigate the effect of matrix constituents. The ECC also utilizes steel fibres along with PE fibres to improve the sustainability index, which is further validated through an environmental impact investigation. Microstructural techniques such as scanning electron microscopy (SEM) and X-ray diffraction (XRD) analysis are also utilized to analyse the associated mechanism to insightfully understand the decomposition stages of PE fibre, microcracks development in different binder systems, and influence of water quenching on the hydration products at different temperature range.

2. Experimental programs

2.1. Raw materials

The materials used for the development of ECC included general purpose cement, class F FA, GGBFS, dolomite powder, SF, local dune sand passing through 300 μm, poly-carboxylic ether based high range water reducer (HRWR) and tap water. The chemical composition and other properties of the binder material were similar as adopted by Rawat et al. (2022). PE fibre with length 12 mm, aspect ratio 500 and steel fibre with length 13 mm, aspect ratio 65 were used to design the hybrid ECC.

2.2. Mix designs

Five different types of mixes were considered with varying fibre content or matrix ratio as highlighted in Table 1. The main mix (M1) is the optimal mix containing GGBFS, fly ash and dolomite which was obtained after the application of weighted Taguchi method with utility concept in authors' previous work (Rawat et al., 2022). This mix demonstrated excellent compressive and tensile performance with compressive strength >100 MPa, peak compressive strain >0.5%, elastic modulus >35 GPa, tensile strength >10 MPa, and ultimate tensile strain >2%. In addition, four other mixes (M2 to M5) are also considered to study the effect of the SCM and fibre content.

The main difference between M1 and M2 is the content of dolomite. M1 had 15% dolomite (by weight of cement), whereas it was 10% in M2. Dolomite (calcium magnesium carbonate) was mainly chosen due to its unique thermal decomposition process with magnesite component releasing CO_2 at ~300 °C and CO_2 from calcite component evolving between 700°C and 900 °C (Olszak-Humienik and Jablonski, 2014). This decomposition may have the potential to partially resist the temperature rise. Furthermore, all fly ash and dolomite were replaced by GGBFS in M4 keeping the total binder content constant to explicitly analyse the effect of GGBFS. To study the effect of fibre content on the residual compressive performance of ECC, the ratio of steel and PE fibres is varied in M3. Volume of PE and steel fibres was changed from 1.5% to 1.25% and 0.75% to 1%, respectively. In addition, the matrix composition of mix M5 has only cement and silica fume as adopted in Zhang et al. (2021b) with fibre content same as M1. This was chosen to analyse the effect of type of matrix constituent on the residual compressive performance. All the considered mixes achieved ultimate tensile strain >2% with clear strain hardening behaviour.

2.3. Specimen preparation and test methods

Cylinders of 75 mm in diameter and 150 mm in height were used to assess the compressive behaviour of the mixes at elevated temperatures. The specimens were mixed in 100-litre mixer with rotating shaft using the procedure stated in Rawat et al. (2022) and cured at standard curing condition in fog room (23 ± 1 °C and 95 ± 5% relative humidity) for 28 days. At the end of the standard curing period, the samples were moved to and kept in an environmental room at 20 °C and 55% relative

Table 1
Mix proportions used in this study.

Mix ID	Binder				Sand	Water	HRWR	PE	Steel
	Cement	GGBFS	FA	Dolomite					
M1	1	0.94	0.19	0.38	0.91	0.50	0.05	1.50%	0.75%
M2	1	0.83	0.17	0.22	0.81	0.44	0.04	1.50%	0.75%
M3	1	0.94	0.19	0.38	0.91	0.50	0.05	1.25%	1%
M4	1	1.00	0.00	0.00	0.73	0.40	0.04	1.50%	0.75%
	Cement	Silica fume	FA	Dolomite	Sand	Water	HRWR	PE	Steel
M5	1	0.11	0.00	0.00	0.44	0.22	0.02	1.50%	0.75%

Note: All ratios are expressed as weight proportions of cement content except the fibre content which is expressed as volume fraction of the mix.

humidity for another 28 days to remove any excess moisture to minimize the impact on the actual testing. Thereafter, the surface of the cylinder specimens was smoothened by grinding from both sides and the specimens were then tested at elevated temperatures.

2.3.1. Testing program at elevated temperatures

Three types of variations were considered to carefully analyse the effect of the testing parameters including the effect of air cooling, water cooling and pre-drying.

a) Effect of air cooling

In this case, the specimens were heated to 200, 400, 600, and 800 °C after the completion of curing. The heating rate was maintained at 1 °C/min to reduce any chance of spalling so that the effect of matrix constituents and fibre ratio can be effectively studied. The specimens were kept at the target temperature for 2 hours (h) and then were allowed to cool by turning off the furnace until the ambient temperature was reached (Fig. 1a).

b) Effect of water cooling

The main difference in this case was the type of cooling after exposure to elevated temperatures. The specimens were first exposed to 200–800 °C under similar condition as case a) and then were quickly dropped into water for cooling. The general heating profile for both conditions is shown in Fig. 1. The temperature of water for quenching was maintained in the range of 22–25 °C through a continuous water flow so that a uniform condition of water quenching can be achieved. Samples were taken out from water after 30 min and then were allowed to surface dry for 24 h before performing the compressive tests.

c) Effect of pre-drying

In this case, specimens were first put into an oven at 90 °C to undergo a pre-drying treatment for 7 days. This temperature was recommended by Liang et al. (2018) to avoid any change in microstructure as a result of pre-drying. After pre-drying is completed, specimens were then exposed to different temperature regimes similar to case a) and thereafter, were naturally cooled in the air. Fig. 2 depicts the temperature profile used for this condition.

2.3.2. Mechanical test program

Uniaxial compression tests were conducted as per ASTM C39 (ASTM-C39, 2012) to obtain the stress-strain curve for both control specimen (at ambient temperature) and specimens at elevated temperatures. A 3000 kN capacity compression testing machine was used to conduct the compression tests at a displacement rate of 0.05 mm/min. For each set of mix, at least three specimens were tested under compression to obtain a statistically consistent average. Elastic modulus tests were also carried out on the same machine in accordance with ASTM C469 (ASTM-C469, 2014) at a loading rate of 0.25 MPa/s. Further details about the test arrangement and measurement method can be

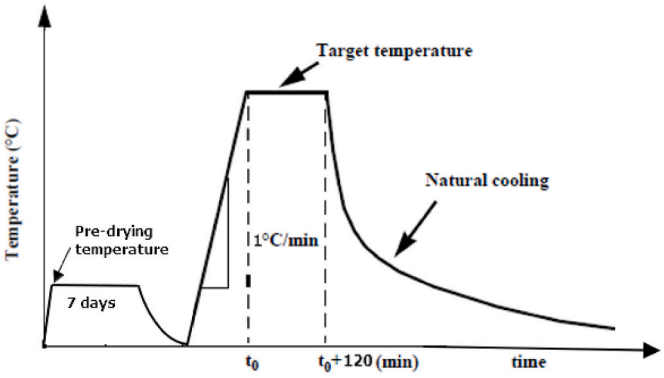

Fig. 2. General heating profile for residual tests with pre-drying treatment.

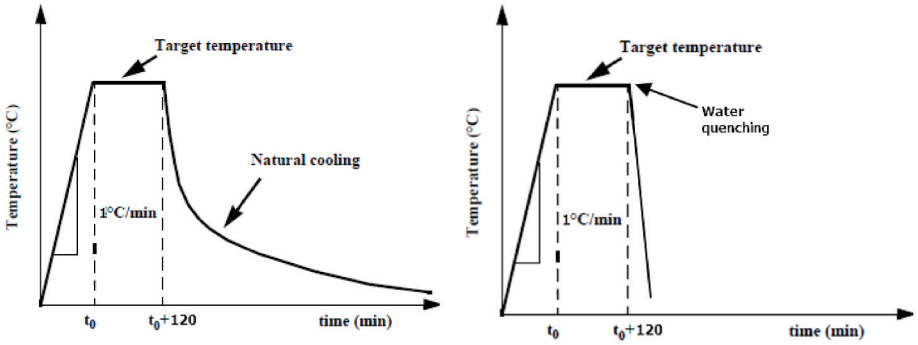

(a) Air cooling **(b) Water cooling**

Fig. 1. General heating profile for (a) air cooled (b) water cooled residual compressive tests.

found in the authors' previous work (Rawat et al., 2022). A total of 340-cylinder specimens were tested, 150 of which were used to analyse the effect of air cooling and the rest were used to investigate the effect of pre-drying and water quenching. The general notation used to denote the specimen is 'Mx-X-Y or M1-X', here Mx is the mix ID, x = 1,2 … 5, X is the exposure temperature ranging from 20°C to 800 °C, and Y denotes the type of elevated temperature testing namely AC, OD or WC, where AC - air cooled, OD – oven dried and WC – water cooled.

2.3.3. Microstructural test program

SEM and XRD analysis were employed to examine the morphology of ECC mixes, fibre state and crack patterns to obtain better understanding of residual compressive properties after exposure to the elevated temperatures. After the compression testing, small samples were collected from the core of specimen of each set and were dipped in acetone for at least 48 h to stop further hydration and dried at 60 °C for another 24 h. Thereafter, part of the sample was used for SEM analysis and the rest of the sample was ground into fine powder of size <300 μm for XRD analysis.

To image the microstructure, solid samples were carbon coated and then analysed using a Phenom XL SEM with an accelerating voltage of 15 kV and 1 Pa chamber pressure. The elemental composition of samples was further correlated using the Phenom energy dispersive spectroscopy (EDS) system. XRD patterns were obtained using a Bruker D8 Advance XRD with a tube accelerating voltage and current of 40 kV and 40 mA, respectively. Powdered samples were mounted in a Bruker back-loading sample holder and scans were carried out across 5–80° 2θ, with a step size of 0.02° 2θ and counting time of 2.5 second per step.

3. Results and discussions

3.1. Residual compressive strength

Table 2 shows the average compressive strength of all the mix specimens at ambient temperature and after exposure to temperature ranging from 200 to 800 °C under air cooling. The control compressive strength varied from 138.1 to 153.7 MPa with the highest being for the mix M5 with silica fume. Among M1 and M3 with only difference in the fibre volume, M3 had higher compressive strength due to the presence of higher volume of steel fibre. Steel fibres can create a spatial network structure that can efficiently absorb energy and impede the spread of cracks under stress, leading to increase in compressive strength (Ren et al., 2022).

As further highlighted in Table 3, compressive strength suffered continual decrease with increase in temperature from 20 to 800 °C. Nevertheless, the reduction was not significant till 200 °C. All the specimens were able to retain more than 85% of the room temperature strength at this temperature. This decline in compressive strength between 20 and 150 °C relates to the loss in the cohesion of the van der Waals forces between the CSH layers. As a result, the surface energy of the CSH layers decreases leading to the formation of silanol groups with weaker bond strength (Dawood et al., 2020). However, this change only has superficial impact and therefore, there was no significant reduction at 200 °C. Thereafter, the compressive strength decreased due to the decomposition of calcium hydroxide (CH) at 430–600 °C and transformation of CSH to C_3S at around 560–600 °C (Rawat et al., 2021).

Table 2
Average compressive strength of ECC at different temperature exposure.

Mix ID	Compressive Strength (MPa)				
	20 °C	200 °C	400 °C	600 °C	800 °C
M1	138.1	121.3	106.9	95.7	53.0
M2	142.4	134.8	113.8	94.00	59.6
M3	145.2	122.5	108.3	102.49	46.6
M4	143.7	131.7	119.1	108.2	58.3
M5	153.7	139.1	98.1	87.4	34.6

Note: The 20 °C strength is reported from the first batch of testing. For each batch, the control specimens were separately tested, and the relative comparison is then drawn through the respective normalised value.

Fig. 3 shows the normalised compressive strength of ECC mix at different temperatures with error bars. The normalised strength has been calculated as the percent retained strength at the reference temperature with respect to the strength of the unheated specimens of the same batch. It can be observed that compressive strength shows a linearly decreasing trend till 600 °C and takes a sharp drop at 800 °C. The transformation of α-quartz to β-quartz or complete decomposition of CSH may have been the cause of this sharp change (Way and Wille, 2016). The mix containing silica fume suffered the largest decrease in compressive strength with just 25% strength retention at 800 °C possibly due to the presence of thermally vulnerable matrix. All other mixes with dolomite and GGBFS (M1, M2 and M4) showed lesser decrease in strength and the retained strength at 800 °C was around 44–48%, signifying that the type of binder can significantly contribute to the post-fire strength retention. Furthermore, the influence of fibre content was distinctly evident as the matrix containing lesser PE fibres (M3) displayed greater damage with only 38% strength retention. This could possibly be attributed to the presence of large thermal stresses in M3 specimens. Higher amount of PE fibres would result in improved dissipation of pore pressure, consequently reducing the likelihood of matrix degradation as observed for M1.

Fig. 4 further shows a comparison of the obtained residual strength of M1 and M4 specimens with the exisitng study on PE fibre based ECC and international standards such as Eurocode 2 (EN, 1992-1-2, 2004) and ACI 216 (ACI 216.1, 2014). Note that for the clarity of the plot, no error bar is shown in Fig. 4. It can be noticed that both M1 and M4 mixes are able to retain higher strength than the previous reported values and this difference is much higher after 400 °C. Therefore, it can be affirmed that the proposed matrix blend is very effective in restricting the damage at higher temperature exposure.

3.1.1. Effect of predyring

The overall trend of the decline in residual compressive strength for oven-dried specimens (with error bars) was the same as the air cooled specimens with a slight difference in the percentage decrease (Fig. 5). Residual strength reduced to 87–92% of the original compressive strength at 200 °C, 66–78% at 400 °C, ultimately reducing to 52–75% at 800 °C. The highest percentage decrease was observed in M5 specimens which was similar to the trend observed after air-cooling.

Fig. 6 further shows a comparison of the residual strength of ECC specimens as a ratio of oven-dried to air cooled (Again, for clarity purpose, no error bar is shown.). It can be observed that only around

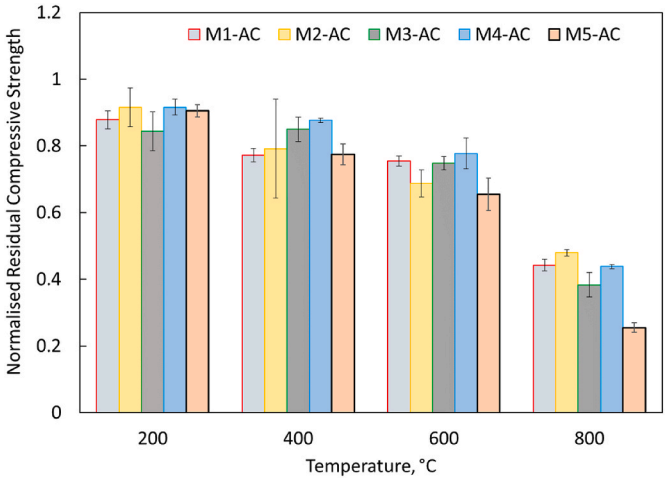

Fig. 3. Normalised residual compressive strength of ECC mixes.

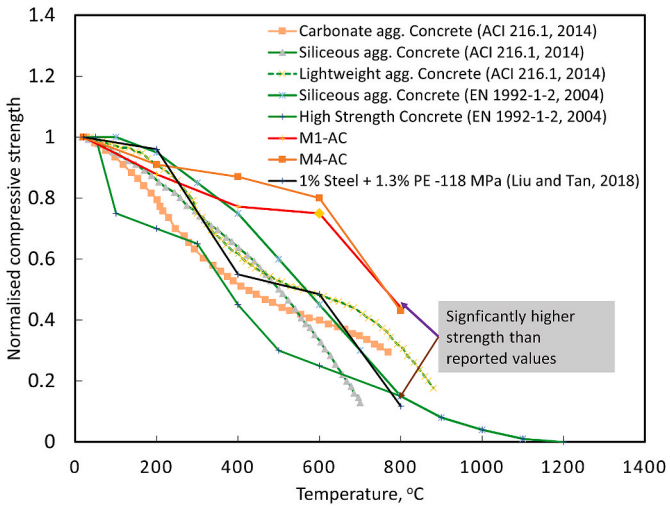

Fig. 4. Comparison of residual strength of ECC mixes with exisitng litearture

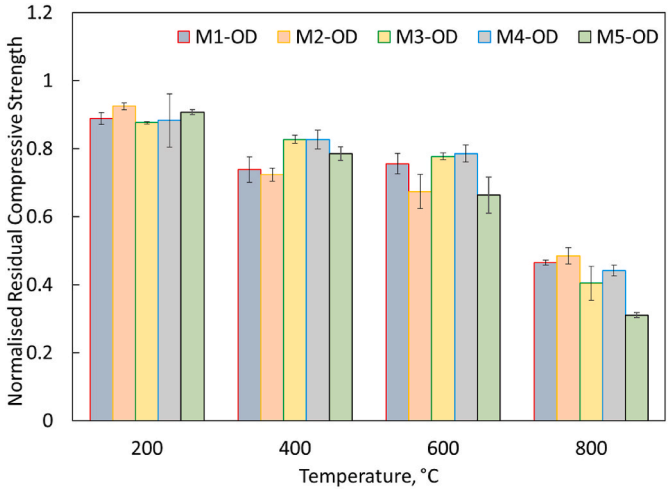

Fig. 5. Normalised residual compressive strength of ECC mixes after pre-drying treatment.

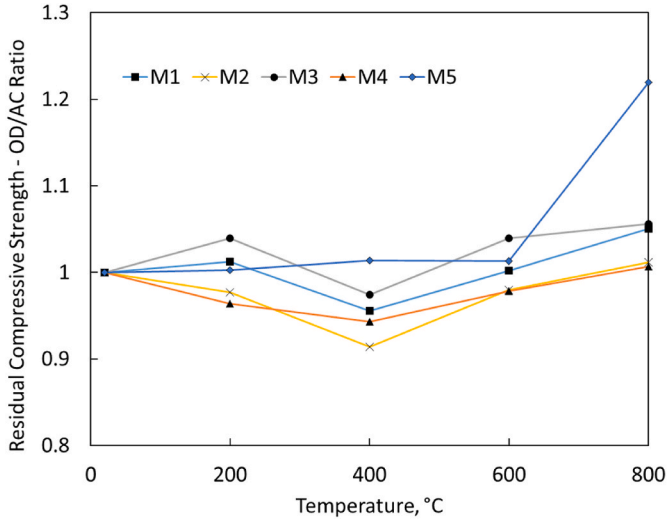

Fig. 6. Comparison of residual compressive strength as a ratio of pre-dried to air cooled condition.

0.05–1% increase was observed in the residual compressive strength of the oven dried specimens especially till 600 °C which becomes negligible if the standard deviation of the data is considered. Strength retained at 800 °C for M5 was 25.5% for the air-cooled specimens, whereas it was 31.1% for the oven-dried specimens. However, the increase at 800 °C was not as noticeable for other mixes as mix M5 and therefore, it may be biased to directly relate this increase to the effect of oven drying. Overall, though the procedure of pre-drying may lead to a partial improvement in the strength, it may not necessarily be important in driving the change in the overall performance and hence can be omitted if desired.

3.1.2. *Effect of water cooling*

Fig. 7 shows the variation of the compressive strength (with error bars) of the ECC specimens after undergoing thermal expsoure and subsequent water cooling. In general, the percentage decrease for water cooled specimens was more than the air cooled specimens which may have been due to the impulsive effect of thermal shock casued by quenching. For instance, the compressive strength reduced to around 87.8% of the control value at 200 °C for air cooled specimen, whereas the strength retention for water cooled specimens was 71.8% for M1 mix specimens. The strength of all water-cooled specimens significantly reduced at 800 °C. The residual compressive strength for air cooled and water cooled M1 mix specimen was 44.2% and 28.6%, respectively at this temperature. This severe degradation was consistent for all mix types resulting into a strength loss of around 67–78% at 800 °C with mix M5 showing the highest decrease.

Relative effect of cooling can be further visualised from Fig. 8 which shows a comparison of the residual performance of ECC specimens as a ratio of water cooled to air cooled strength. A comparison has also been provided with the data from the exisitng literature (Shang and Lu, 2014; Li et al., 2019b; Yu et al., 2015; Yu et al., 2014). It can be observed that water cooling has an adverse effect at 200 °C with the strength of water cooled specimens falling by approximately 20% with respect to the air cooled specimens. The negative effect of water cooling was less pronounced in the temperature range 400–600 °C in all mixes, which may have been due to the onset of rehydration. The residual compressive strength for water cooled specimens (with respect to air cooled specimens) increased between this temperature range and even reached closed to or a little higher than 1. Water cooled specimens had severe degradation at 800 °C in comparison to the air cooled specimens as shown in Fig. 8 (Again, error bars are excluded for clarity of the comparsion.). It should further be noted that the overall trend was consistent for all mix types irrespective of type of matrix or fibre content. However,

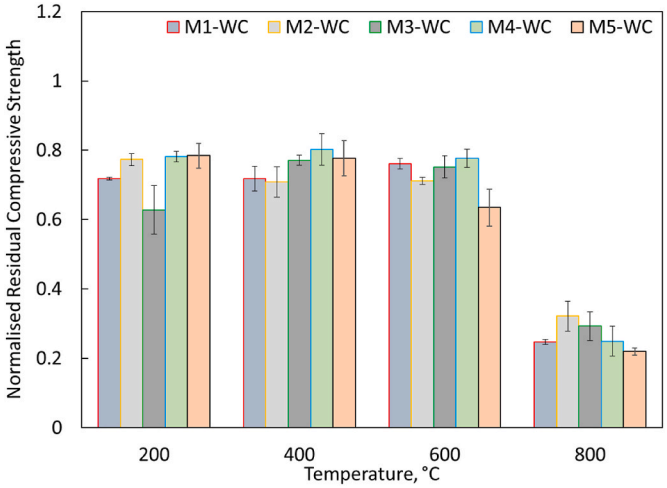

Fig. 7. Normalised residual compressive strength of ECC mixes after water cooling.

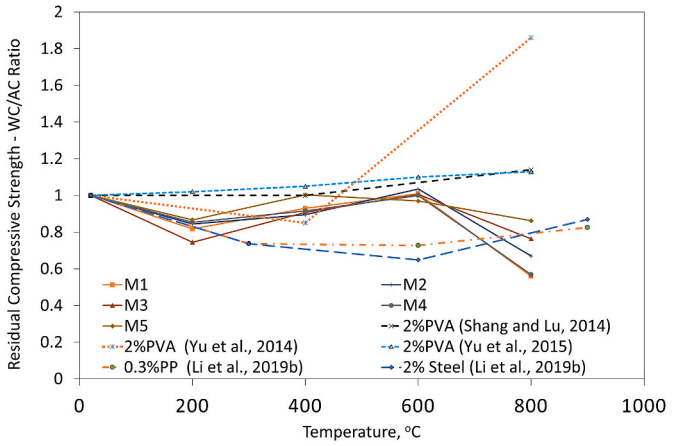

Fig. 8. Comparison of residual strength of ECC as a ratio of water cooling to air cooling.

the trend somewhat deviates from that reported in exisitng studies which present conflicting trend. Based on the current observations, it is quite clear that the effect of water quenching jointly depends on the extent of rehydration and the damage caused due to thermal shock. Therefore, the cumulative effect will be dependent on the governing phenomenon between these two and can not be said to be directly dependent on the either of these as reported previously (Shang and Lu, 2014; Li et al., 2019b; Yu et al., 2015; Yu et al., 2014). At 400–600 °C, the posibility of rehydration is much higher which may reduce the negative impact caused by water quenching. However, at very high tempertature of 800 °C, the decomposition of primary hydration products is almost complete and therefore, the rehydration may be overshadowed by the resultant change due to thermal shock and hence, a signfiicant decrease in the compressive strength was observed.

3.2. Compressive stress-strain relationship

Figs. 9–11 illustrate the compressive stress-strain relationship of the air-cooled, oven-dried, and water-cooled specimens at each target temperature. In general, the stress-strain curves comprised of an initial elastic region, a parabolic segment rising to the peak stress and then a descending segment until the data recording is stopped. The actual capture of descending section was not possible for all the specimens due to the irregular control of the machine. Therefore, the post-peak observations are only reported to provide a rough comparison of the behaviour. As previously highlighted, compressive strength decreased, and the stress-strain response became increasingly flatter with increase in temperature especially above 400 °C. This behaviour was consistent for all mix types irrespective of the type of cooling or pre-drying. The presence of steel fibres and its subsequent softening at higher

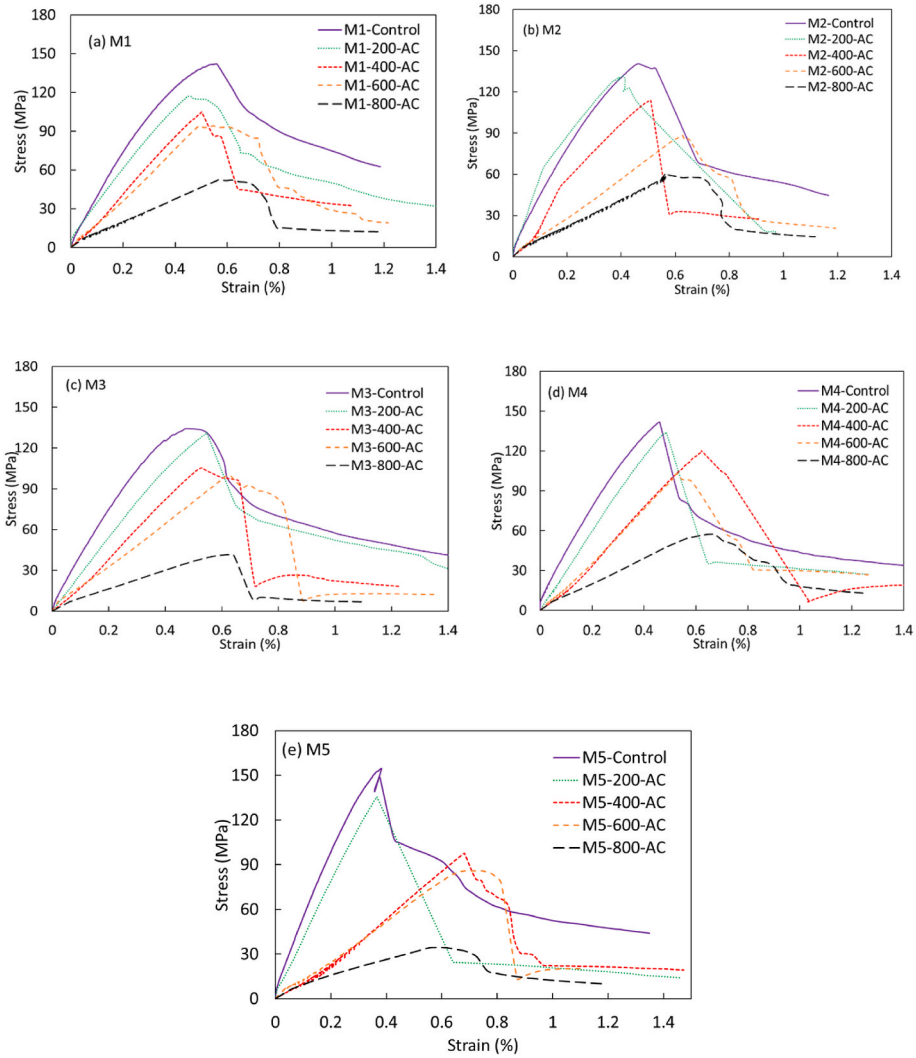

Fig. 9. Residual stress-strain response of ECC mix after air cooling.

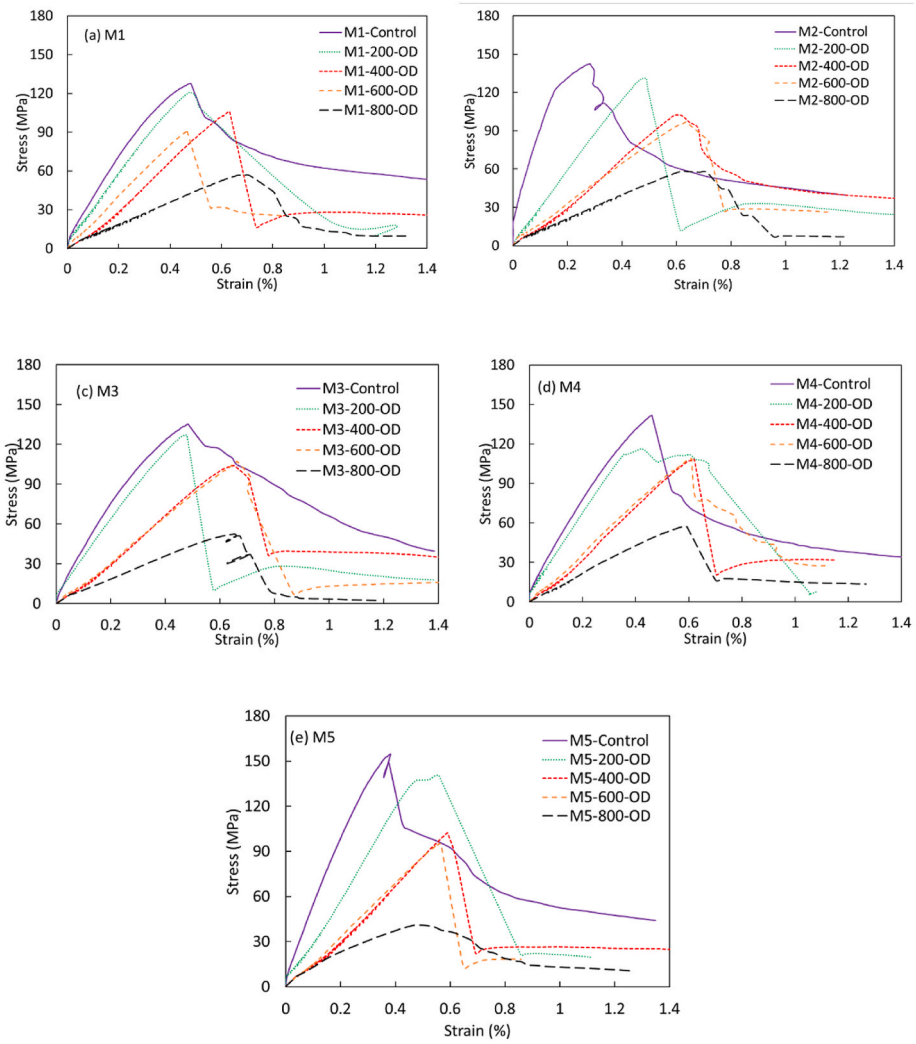

Fig. 10. Residual stress-strain response of ECC mixes after pre-drying treatment.

temperatures may have contributed to this increased ductility.

There was no observable difference in the stress-strain response for the oven-dried specimens and air-cooled specimens. However, the stress-strain response of the water-cooled specimens was relatively flatter, and the flatness increased with increase in temperature. Subsequently, reduction in compressive strength was higher and peak compressive strain increased with temperature. In general, M3 had the highest average peak compressive strain at room temperature, whereas M5 had lowest. The average strains corresponding to peak stress at 800 °C increased by around 1.03–1.37 times and around 1.01–1.29 times to that of the room temperature strain for air cooled and oven-dried specimens, respectively. For the water quenched specimens, strain corresponding to peak stress at 400 °C increased to 0.98–1.42 times the room temperature strain and it further changed to 1.05–1.43 times at 800 °C maintaining a slightly higher value than air-cooled or oven-dried specimens.

3.3. Residual elastic modulus

The room temperature elastic modulus of M1-M5 mix specimens ranged from 36.5 to 38.6 GPa. Fig. 12 highlights the normalised elastic modulus of the air-cooled specimens at different temperature exposure. It should be noted that as variations of different specimens from the same mix are very small, error bars are not included in Fig. 12 for clarity of the plot. It can be clearly noticed that the residual elastic modulus suffered continuous decline with rise in temperature and the loss was significantly high from 400 °C and above due to the melting and vaporisation of fibres. This observation trend is consistent with the existing studies (Rawat et al., 2021).

Similar to the observation of residual compressive strength, it can be seen that the residual elastic modulus is dependent on both matrix constituents and fibre volume. Mix M1, M2, M4 and M5 have similar content of fibres, but different ratio or type of matrix constituents and therefore, suffered different level of deterioration after exposure to elevated temperatures. It is worth noting that the percentage loss in elastic modulus with rise in temperature was higher than that of compressive strength. This is due to its higher sensitivity of elastic modulus to micro-cracks (Sahmaran et al., 2010). Elastic modulus reduced to around 40–60% of the initial value at 400 °C due to the micro-cracks and considerable amount of mass loss at this temperature, both of which are sensitive parameters for stiffness. Highest degradation was observed in M5 with the residual elastic modulus decreasing to 38% of the room temperature value at 400 °C which further reduced to 24% at 800 °C. At this temperature, the pore space and microcracks may have increased, leading to the eventual reduction in strength against deformations (Dabbaghi et al., 2021). Mix M1 and M4 suffered least degradation with an approximate retention of around 25–30% at 800 °C. M3 with a higher amount of steel fibre and low amount of PE fibre showed around 24.9% retention in modulus at 800 °C. This further confirms that the matrix with silica fume is more prone to damage and

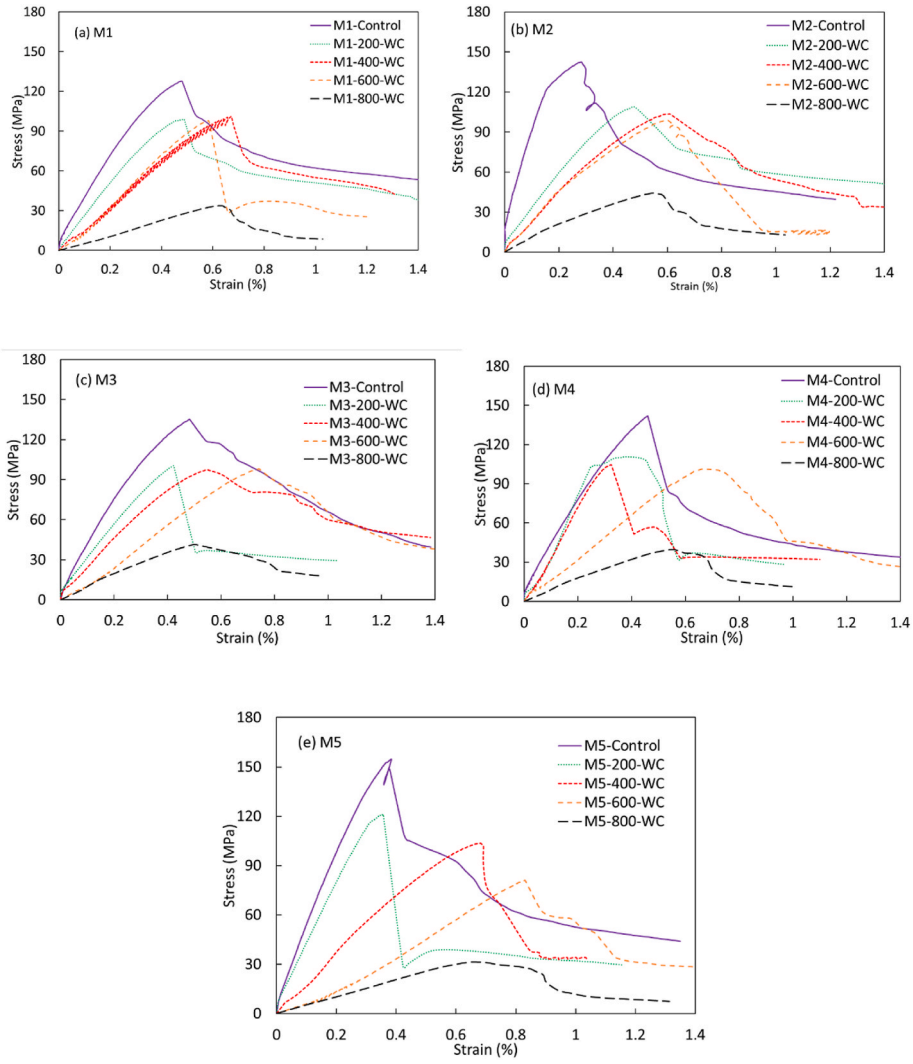

Fig. 11. Residual stress-strain response of ECC mixes after water cooling.

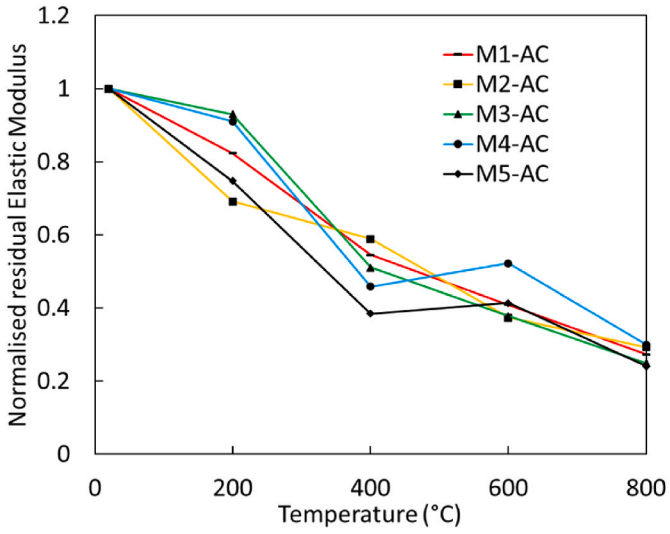

Fig. 12. Residual elastic modulus of ECC mix at different temperatures.

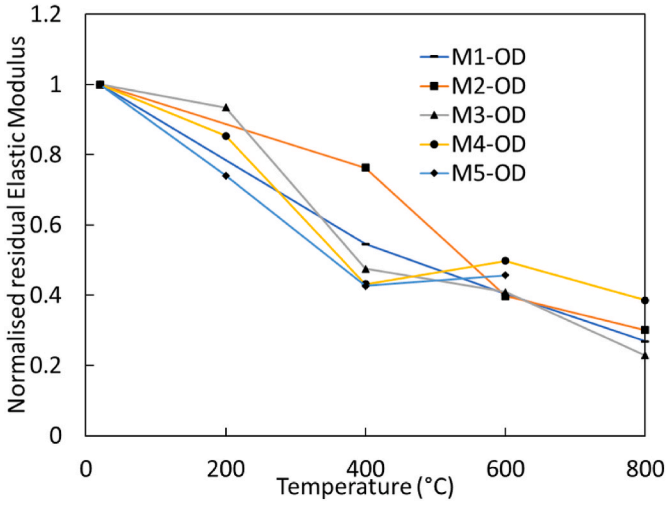

Fig. 13. Residual elastic modulus of ECC mixes after pre-drying treatment.

therefore may result in significant degradation in both strength and stiffness. With the use of better thermally performing SCMs and optimum proportions of fibres, it is possible to improve the residual compressive performance even without changing the fibre type.

3.3.1. Effect of oven-drying

Fig. 13 shows the variation of residual elastic modulus for the M1 to M5 specimens subjected to pre-drying procedure. Similar to Fig. 12, error bars are not shown here as variations of different specimens from the same mix are very small. No significant difference was observed in comparison to the non-dried specimens at all temperature ranges. For instance, the air-cooled specimens had modulus retention of around 27.8% for M1 and 29.3% for M2 at 800 °C, whereas this was approximately 26.8% for M1 and 30% for M2 for the oven-dried specimens at the same temperature. Similar trend can be seen for all other mix types with no clear improvement due to oven-drying. Therefore, it can be concluded that pre-drying of specimens may not lead to any meaningful positive or negative variation in the residual compressive performance (both strength and stiffness) and can be adopted in spalling studies without any reservations regarding the mechanical performance.

3.3.2. Effect of water quenching

Fig. 14 shows the variation of residual elastic modulus with temperature for the specimens subjected to water quenching (Again, error bars are not shown due very small variations of specimens from same mix.). Though the overall trend was similar to the air-cooled specimens, water cooling did not have any severe effect on elastic modulus. In fact, water cooling had more noticeable effect on the residual modulus due to rehydration especially for 400 and 600 °C exposed specimens as shown in Fig. 14b.

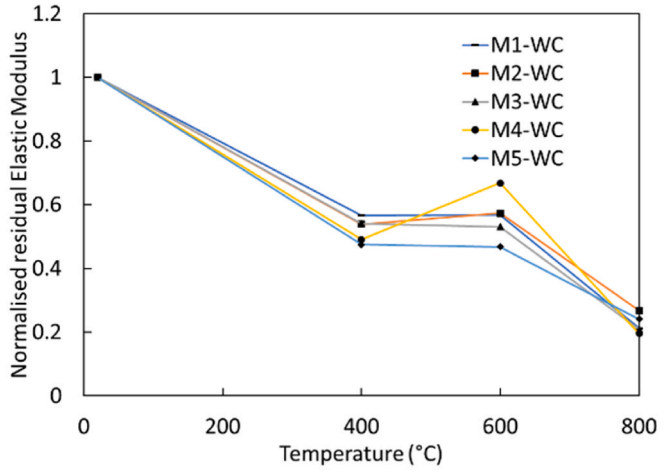

(a) Water-cooled

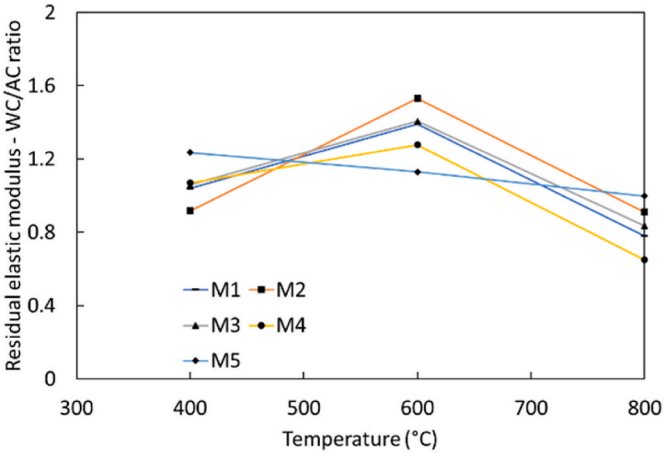

(b) Ratio of WC/AC

Fig. 14. Residual elastic modulus of different ECC mixes after water cooling.

At 400 °C, the water-cooled specimens of mix M1 showed around 56.6% retention in elastic modulus which was around 1.1 times higher than the air-cooled specimens. The higher retention continued till 600 °C and water-cooled specimen had 1.4 times more retention of elastic modulus for M1 mix. This trend was consistent for all the mixes. The difference in percentage change due to water cooling may be associated with the greater sensitivity of elastic modulus on micro cracks and mass loss. With a severe decrease already taken place on air cooling due to the cracks and dehydration, the overall effect due to rehydration may have been more pronounced and therefore, there was a slight increase in the residual modulus on water cooling till 600 °C. This further reconfirms the dependence of the residual compressive performance on the internal damage due to thermal shock and possible rehydration.

4. Qualitative characterisation and microstructural evolution

4.1. Surface damage

A simple way to ascertain the damage occurring due to elevated temperature is through visual identification. Increase in temperature may lead to change in the surface texture of the specimens. On exposure to elevated temperatures, both oven-dried specimens and air-cooled specimens underwent similar change in surface texture as can be seen from Fig. 15. There were no obvious cracks till 400 °C exposure in any type of mixes. However, very fine micro-cracks became apparent after 600 °C exposure which can be ascribed to the rise of thermal stress and onset of matrix degradation. After 800 °C exposure, all specimens suffered microcracks and the intensity of the cracks was more in M4 and M5 specimens. This can further be visualised through Fig. 16 which shows the binary images of M1 to M5 air cooled specimens after 800 °C exposure obtained through ImageJ software.

The crack density can be pictured in form of line network, whereas the black colour is due to either the background noise or melted fibre residue. It can be observed that there were no apparent cracks in M1-M3 specimens containing dolomite. Surface cracks were clearly visible in M4 specimens with minor intensity. However, M5 specimens had severe propagation of cracks throughout the surface area which highlights the negative effect of its matrix constituents.

For the water quenched specimens, the texture slightly differed from the air-cooled or oven-dried specimens especially after 400 °C. Water cooling may significantly affect the outer surface in terms of appearance and therefore, the cracks were more apparent even though there was no significant change in the strength at this temperature as explained previously. Nevertheless, no spalling was observed in any of the specimens indicating the effectiveness of PE-steel fibre hybridization. This may also have been due to the adopted low heating rate and smaller specimen size.

4.2. Stages of PE fibre melting at elevated temperatures

Figs. 17–18 show the SEM micrographs obtained for the samples from mix M1 and M5 after exposure to 200–600 °C. After 200 °C exposure, vacant channels can be consistently observed in all the sample types due to the melting of PE fibres. However, black residue was noticed in these channels as the melted PE fibres were still present. The decomposition temperature of PE fibre is 495 °C which is much higher than the exposure temperature 200–400 °C. Therefore, the channels are found to be completely free of carbon residue only after 600 °C exposure in all types of mixes irrespective of the type of binder. Despite this, PE fibres still played a reasonable role in mitigating the damage and hence,

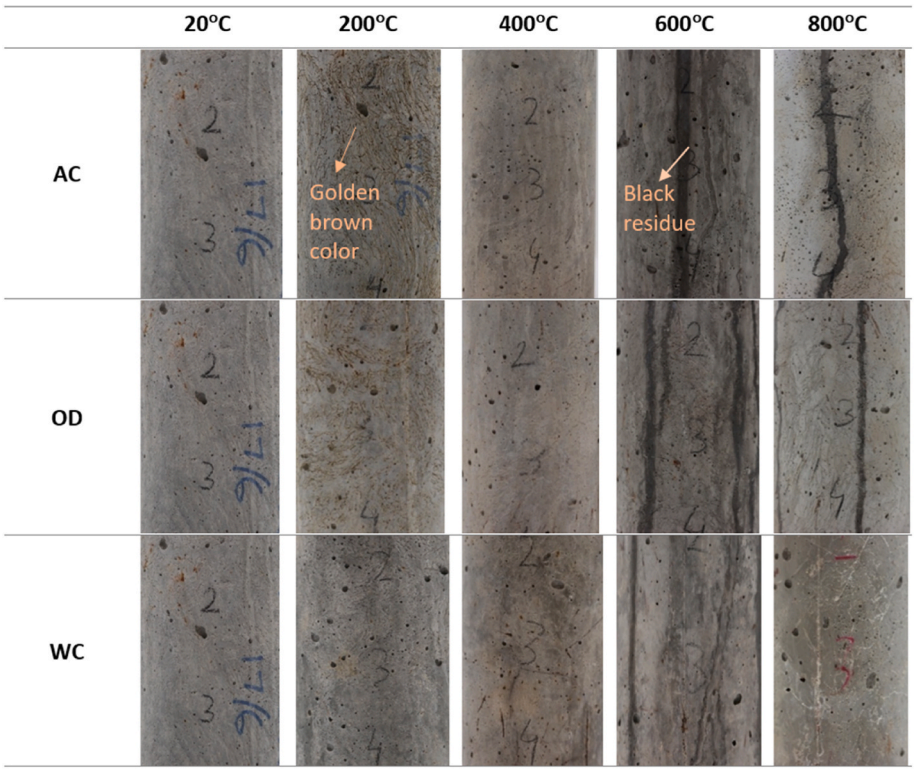

Fig. 15. Surface of heated M1 ECC specimens.

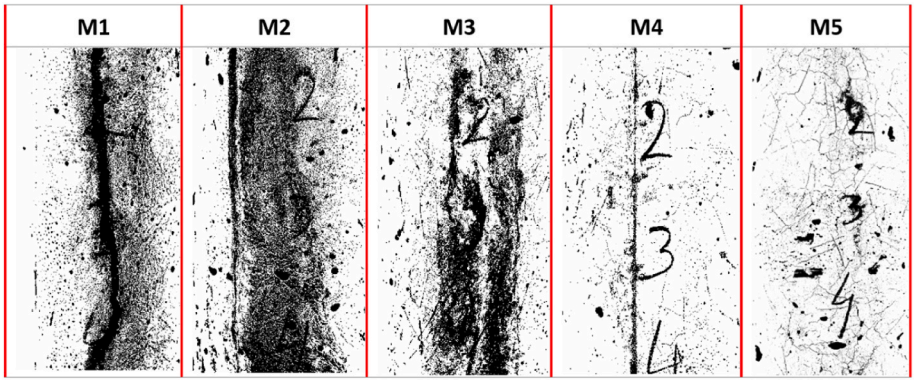

Fig. 16. Binary images showing crack distribution in air cooled 800 °C exposed ECC specimens.

the effect of their melting in resisting the build-up of pore pressure cannot be completely neglected.

4.3. Role of matrix constituents under elevated temperature

Considering the high compressive strength of all mixes at room temperature, it is expected that the microstructure will be dense with fewer unhydrated particles. Therefore, the major difference at elevated temperatures will stem from the ability of material to resist high temperature which may result in lesser microcracks and stable hydration phases. This can further be confirmed through Fig. 19 which shows SEM micrographs of mix M1, M4, M5 after exposure to 600 °C. Calcium compounds (oxides and carbonates) can be clearly seen occupying the space in the M1 samples; however, the overall microstructure remained dense with low observed porosity. Both M4 and M5 matrix also showed dense microstructure with the presence of different forms of calcium silicates. However, microcracks can be clearly observed in M5 especially near the vacant channels which may have been the cause of strength degradation.

Fig. 20 further shows the X-Ray diffractograms of M1, M4 and M5 specimens at different temperatures after air cooling. The main hydration peaks as seen in the M1-control (ambient temperature) was of portlandite (18.04°, 34.11°, 47.13°), dolomite (30.97°), and calcite (29.45°). Mix M4 and M5 also showed similar peaks (except dolomite) at room temperature. Moreover, unhydrated cement constituents namely alite and belite were also observed in all the mixes at room temperature between 26.7-28° and 31–33°. This indicated that complete hydration had not taken place. In fact, these peaks were more apparent in mix M4 and M5. All the peaks remained stable in 200 °C exposed specimens indicating no apparent decomposition of any of the hydration products. Furthermore, portlandite decomposition followed similar trend in all the mixes with intensity lessening on increase in temperature and disappearing above 600 °C.

The main difference was in the peaks of dolomite and alite-belite. In mix M1, peaks of dolomite reduced at 600 °C and flattened at 800 °C indicating that dolomite had decomposed (Fig. 20a). Subsequently, the

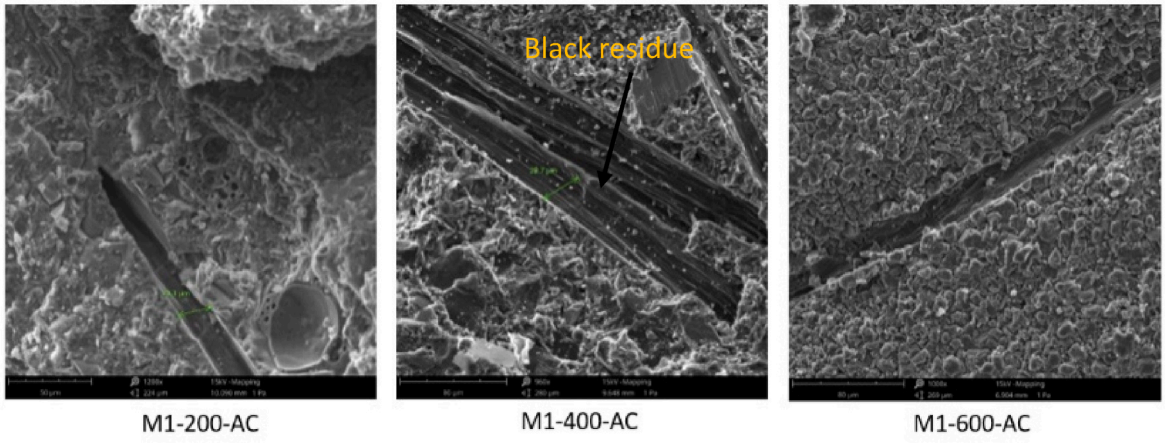

Fig. 17. SEM micrographs of M1 samples at different temperature.

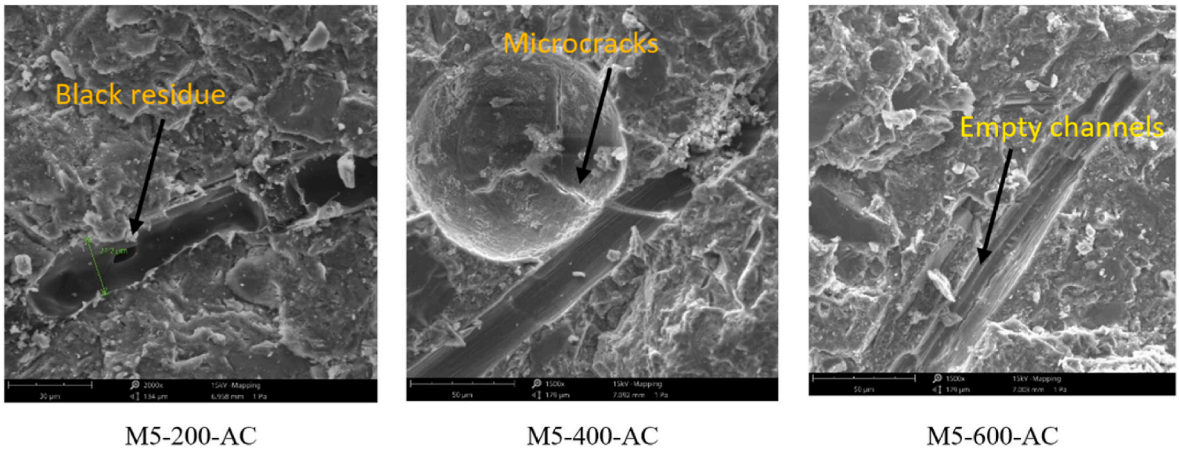

Fig. 18. SEM micrographs of M5 samples at different temperature.

peak of calcite became more evident beyond 600 °C. It is important to note that this decomposition of dolomite results in release of carbon dioxide (as shown in Equations (1) and (2) (Olszak-Humienik and Jablonski, 2014)) which may help in resisting the temperature rise in addition to formation of calcite filler and control the rate of decomposition. This may have been the reason of the higher residual compressive strength of M1.

$$CaMg(CO_3)_2 \leftrightarrow CaO + MgO + 2CO_2\ (> 528^oC) \quad (1)$$

$$CaCO_3 \leftrightarrow CaO + CO_2\ (> 845^oC) \quad (2)$$

Moreover, the peaks of alite and belite remained similar as control specimen till 600 °C in both M1 and M4 (containing GGBFS blends) showing that decomposition did not fully start. With further increase in temperature (at 800 °C), these peaks became clearly apparent indicating decomposition of the main hydration products which may have led to a sharp decrease in the strength.

In comparison, the peaks of alite and belite were more obvious in M5 at 800 °C (Fig. 20c) showing that the overall intensity of the unhydrated particles may be more. This could have contributed to a greater decrease in strength, as evidenced by compressive strength tests. Moreover, the calcite peak also disappears in the M5 specimens at 800 °C as opposed to M4 and M1. This again confirms higher decomposition rate in M5 specimens and subsequently lower compressive strength.

4.4. *Effect of water cooling*

Conflicting observations have been reported in the previous studies regarding the role of water cooling on the performance of ECC. The residual compressive strength and elastic modulus results obtained in the present study shows that the overall effect of the water quenching is dependent on the governing effect between thermal shock and rehydration. This can further be visualised from Fig. 21 which shows the comparison of micrographs of M1 air cooled and water cooled specimens at 600 °C. While the air-cooled specimens showed decomposed products, rehydration products can be seen forming in the voids of the water-cooled specimens which may have caused a partial rise in strength.

Fig. 22 depicts two different micrographs of water cooled M5 mix specimens with one highlighting microcracks (Fig. 22a) or the decomposed products (Fig. 22b) and the other highlighting the onset of rehydration. Therefore, it is quite clear that water quenching may lead to both rehydration and thermal shock and the overall effect is dependent on the dominant mechanism out of these two depending on the temperature range. This governing effect is significantly affected by the matrix composition and therefore, the property of binder plays an important role in determining the elevated temperature behaviour.

The occurrence of rehydration may be further confirmed with X-ray diffractograms. To provide a comparison, the XRD curves of M1 specimens undergoing air cooling and water quenching after exposure to 600 °C has been shown in Fig. 23. The primary difference in peak formation was observed within the range of 30–50° 2θ, hence, only this

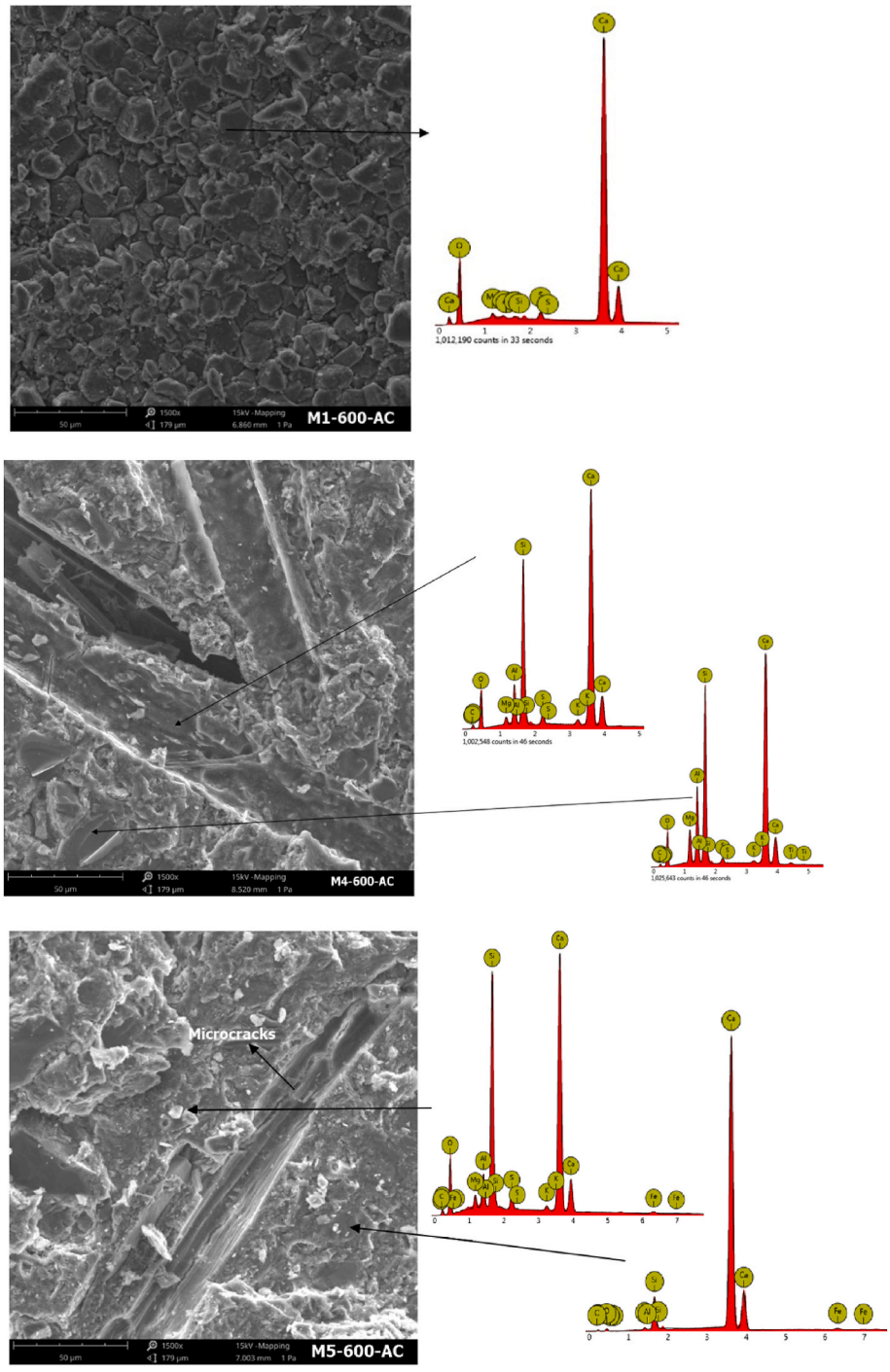

Fig. 19. SEM micrographs of M1, M4 and M5 samples at 600 °C.

interval is depicted. The peaks of major unhydrated compounds, alite and belite seemed to reduce or disappear on water cooling of specimens which may have contributed to rehydration. However, the amount of rehydrated products are not easily distinguishable as they may not have been detected by XRD due to their low intensity.

5. Environmental impact assessment

The current study focused on the development of green ECC while simultaneously achieving high compressive performance at both ambient and elevated temperatures. Unlike the conventional mix which utilizes high volume of ordinary Portland cement (OPC) for PE-fibre reinforced ECC (mix M5), the emphasis was kept on utilization of blends of GGBFS, fly ash and dolomite powder. Moreover, local river sand was utilized instead of the traditional silica sand to further reduce the carbon footprint and cost.

To further analyse the embodied CO_2 emission (ECE) and embodied energy consumption (EEC) for the developed mixes, the respective values of each mix component have been collated from the literature and presented in Table 3. ECE and EEC respectively represent the total CO_2 emission and the total energy required in various stages from production to fabrication throughout the entire lifecycle of a material. It can be seen that substituting river sand for manufactured sand results in significantly lower ECE and EEC. Moreover, the effective utilization of hybrid

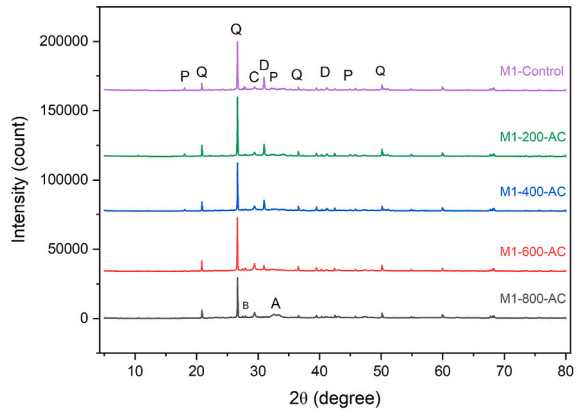

(a) Mix M1

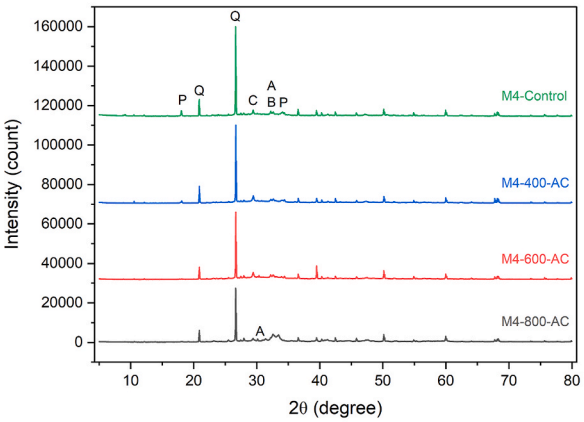

(b) Mix M4

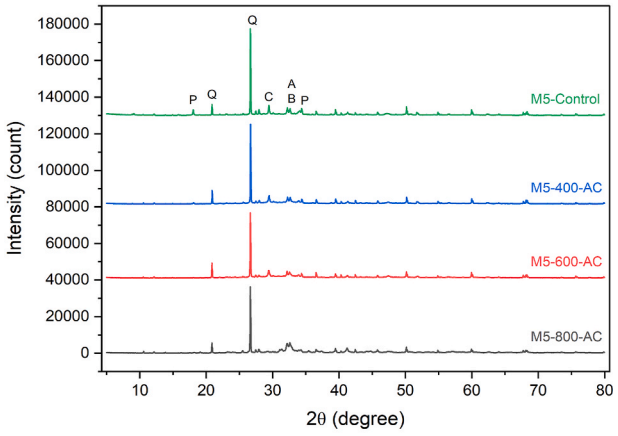

(c) Mix M5

Fig. 20. XRD curves of (a) M1; (b) M4; and (c) M5 mix at different temperatures. [Note: A – Alite, B – Belite, C – Calcite, D – Dolomite, E – Ettringite, Q – Quartz, P – Portlandite].

steel-PE fibre further contributed to reducing the overall environmental impact. Opting for solely PVA or PE fibre, as typically done, would have significantly increased the composite's EEC, given their individual EEC values are nearly double to that of steel. Therefore, the choice of ingredient clearly demonstrates the environmental benefits associated with the developed ECC.

The ECE and EEC of the composite was further calculated by taking the summation of the emission and embodied energy of all raw materials (Fig. 24). These indices can serve as indicators to evaluate the effectiveness of the mix in reducing environmental impact. In addition, another index Normalised ECE (NECE) was also assessed which represents the total embodied carbon emission in one cubic meter of mix emitted to achieve 1 MPa of observed strength.

It can be observed from Fig. 24 that Mix M1 performed better than the conventional Mix M5 across all indices, displaying a significantly lower value (approximately half). Mixes M2, M3, and M4 also show similar performance, with great decrease compared to M5 in all indices. This suggests that the incorporation of dolomite powder and GGBFS blends not only improves performance but may also be economically feasible for producing ECC. In addition, mix M1 shows comparable NECE to M3 despite having slightly high amount of PE fibre. This further indicates that optimizing the fibre ratio is important to achieve best performance in terms of sustainability and mechanical performance.

6. Conclusions

This paper utilized high volume of GGBFS blends for the development of green ECC with enhanced compressive performance at ambient and elevated temperatures. A key aim was to address the sustainability concern arising from the extensive use of ordinary Portland cement in existing ECCs. This was achieved through the hybrid use of PE and steel fibres and novel application of different SCMs including GGBFS, dolomite and fly ash replacing 60% of the cement. The research involved testing five different types of hybrid PE-steel fibre reinforced ECC, comparing their compressive performance under ambient condition and residual performance at different temperatures and varying test conditions. Based on the test results, the following conclusions can be drawn.

- Both matrix constituents and fibre content have a considerable impact on performance of ECC at elevated temperatures, and consequently, careful selection is essential for obtaining superior compressive performance.
- Mix M5 with only silica fume as the primary SCM was found to have higher tendency of strength degradation due to the resultant densified microstructure. However, mix with binary (M4) or quaternary (M1) blends of GGBFS showed superior performance in terms of both higher residual compressive performance and lower environmental impact.
- Mix M1 with blends of GGBFS, fly ash, and dolomite and mix M4 with just GGBFS with 1.5% PE and 0.75% steel fibres showed around 45–48% strength retention at 800 °C. These results are significantly higher than the values reported in international standards such as Eurocode 2 (EN, 1992-1-2, 2004) and ACI 216 (ACI 216.1, 2014) and in existing literatures.
- Decreasing the PE fibre content from 1.5% to 1.25% and increasing the steel fibre content from 0.75 to 1% (mix M3) resulted in reduced residual strength with only 38% strength retention at 800 °C. This confirmed that the PE fibres are effective in preventing severe damage in the matrix as a result of their melting.
- Elastic modulus also showed similar trend and had the highest degradation in M5 mix specimens with only 24.14% retention. M3 with a higher amount of steel fibre and low amount of PE fibre showed around 24.9% retention in modulus at 800 °C which was 27.3% for M1 at the same temperature.
- Pre-heating the ECC specimens in oven at 90 °C did not lead to any negative effect on the residual compressive performance of ECC mix. This effect remained consistent for all the mixes with varying ratio of binder or fibre content and hence, this treatment procedure may be adopted in spalling studies without any reservations about its negative effect on the mechanical performance.
- Water quenching was found to be detrimental to the compressive performance. Sudden cooling in water may lead to strength increase due to rehydration or damage due to thermal shock and the overall effect is dependent on the dominant mechanism among these two. The temperature between 400 and 600 °C is found more favorable for rehydration, whereas at 800 °C, the thermal shock and the

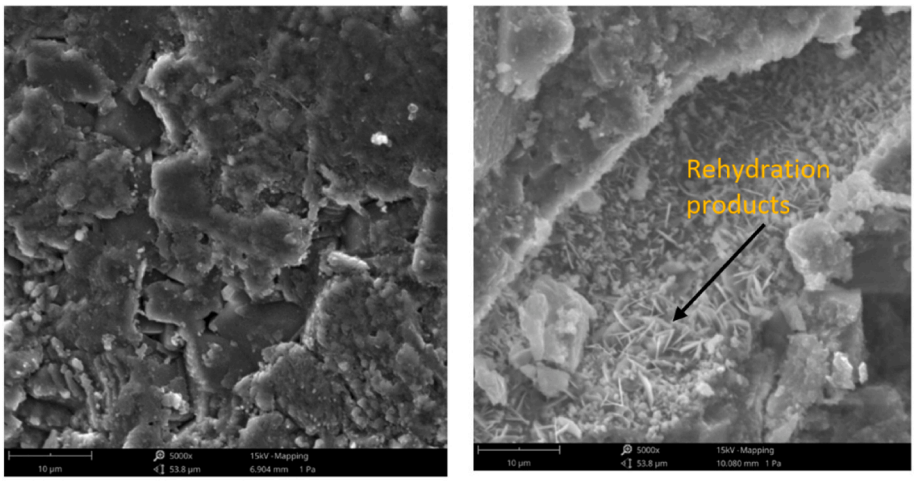

Fig. 21. Comparison of SEM micrographs after air cooling and water quenching for M1 mix after 600 °C exposure.

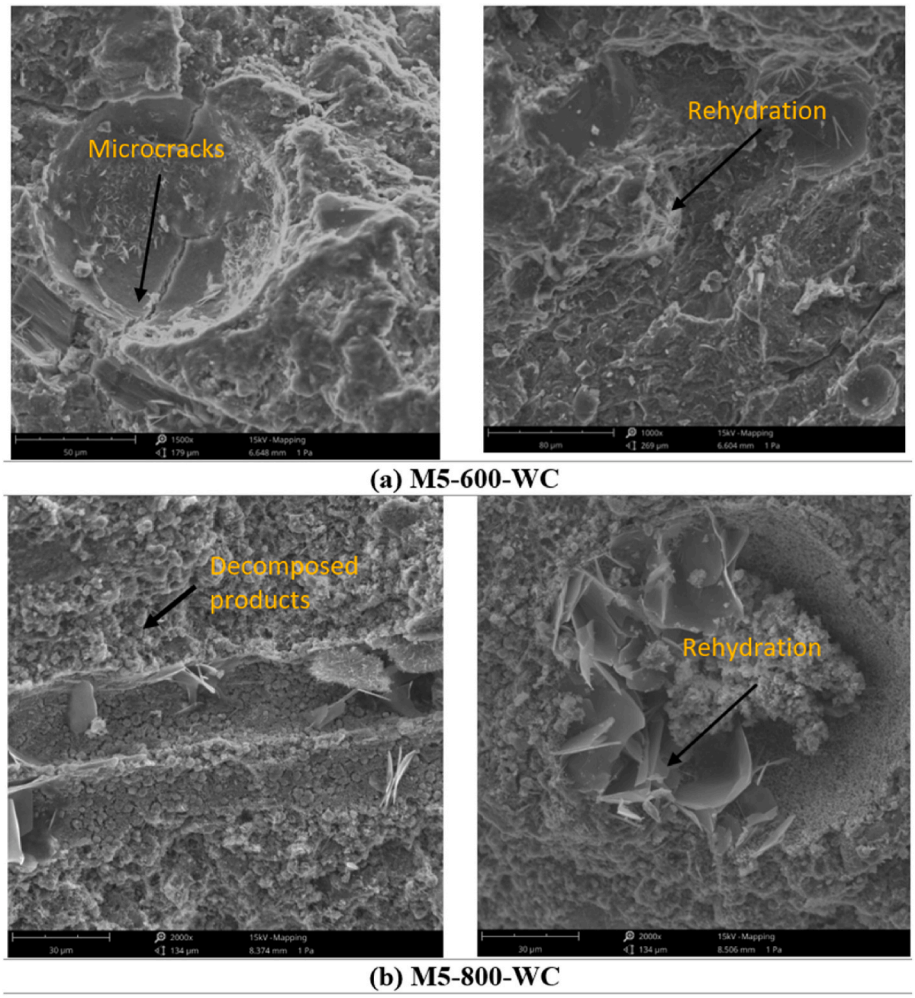

Fig. 22. SEM micrographs of M5 mix after water quenching.

already decomposed microstructure makes it very hard to regain the strength. Moreover, the effect of water quenching was also found to be dependent on the mix constituents with mix M5 with silica fume showing the worst performance.

- The environmental impact analysis further demonstrated the enhanced sustainability of the developed mixes, supported by lower levels of ECE, EEC, and NECE. This was mainly due to the utilization of high volume of SCM (GGBFS, dolomite) as cement replacement. Additionally, the inclusion of fiber hybridization further contributed

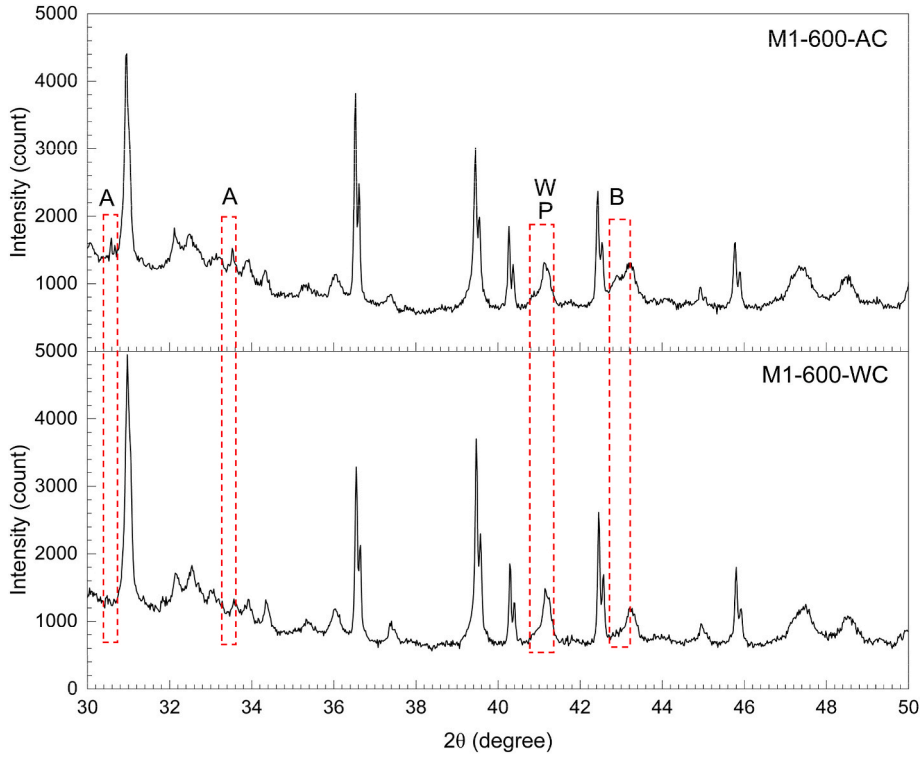

Fig. 23. XRD diffractograms of M1 mix after exposure to 600 °C between 30 and 50° 2θ [Note: A – Allite, B – Belite, P – Portlandite, W – Wollastonite].

Table 3
ECE and EEC of general mix constituents.

Mix constituent		ECE (kg CO_2/kg)	Reference	EEC (MJ/kg)	Reference
Binder	Cement	0.84	(He et al., 2022)	5.75	(Zhong and Zhang, 2021)
	Silica fume	0.15	(Zhang et al., 2024)	0.16	(Zhang et al., 2024)
	GGBFS	0.07	(Zhong and Zhang, 2021)	1.33	(Zhong and.Zhang, 2021)
	FA	0.01	(Taborda-Barraza et al., 2021)	0.1	(Taborda-Barraza et al., 2021)
	Dolomite powder	0.029	(Hu et al., 2023)	0.069	(Hu et al., 2023)
Aggregate	River sand	0.0024	(Shoji et al., 2022)	0.031	(Shoji et al., 2022)
	Manufactured sand (commonly used)	0.023–0.033		0.067–0.226	
Admixture	HRWR	0.75	(Zhang et al., 2024)	11.18	(Zhang et al., 2024)
	Water	0.000196	(Jiang et al., 2022)	0.01	(Xuan et al., 2022)
Fibre	PVA (commonly used)	1.7–3.6	(Shoji et al., 2022)	101–106	(Shoji et al., 2022)
	PE	2		73–116	
	Steel	1.49	(Zhang et al., 2024)	35.3	(Zhang et al., 2024)

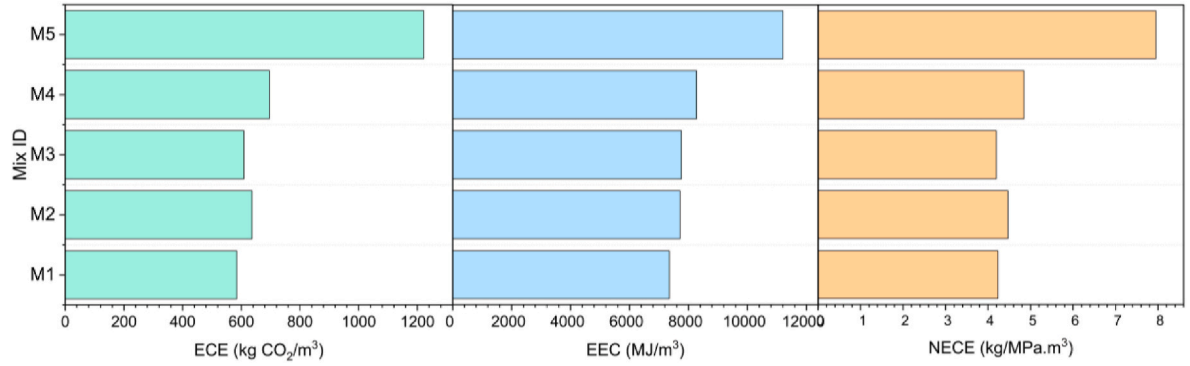

Fig. 24. Environmental impact assessment of the mixes considered in the present study
Note: Water and HRWR were neglected in calculation considering their same quantity among all five mixes.

to reducing the environmental impact due to the significantly lower EEC of steel fibre in comparison to PE fibre. Therefore, it is confirmed that the new hybrid PE-steel ECC with GGBFS, dolomite and fly ash blends (mix M1) does not only exhibits superior perofrmance at both room and elevated temperature but also represents a more sustainable alternative compared to the traditional PE-ECC mix.

CRediT authorship contribution statement

S. Rawat: Writing – original draft, Visualization, Methodology, Investigation, Formal analysis. **Y.X. Zhang:** Writing – review & editing, Supervision, Resources, Conceptualization. **D.J. Fanna:** Writing – review & editing, Visualization. **C.K. Lee:** Writing – review & editing, Supervision, Resources, Conceptualization.

Declaration of competing interest

The authors declare that they have no known competing financial interests or personal relationships that could have appeared to influence the work reported in this paper.

Data availability

Data will be made available on request.

Acknowledgment

Commonwealth's support for this research received through Australian Government RTP and UNSW Canberra's support through UIPA Scholarship are gratefully acknowledged. Partial support from ARC Discovery Project [DP220103043] is also acknowledged. The authors would also like to thank the Advanced Materials Characterisation Facility (AMCF), Western Sydney University for access to instrumentation, staff, and training.

References

ACI 216.1, 2014. Code Requirements for Determining Fire Resistance of Concrete and Masonry Construction Assemblies. American Concrete Institute.
ASTM-C39, 2012. Standard Test Method for Compressive Strength of Cylindrical Concrete Specimens. ASTM International.
ASTM-C469, 2014. Standard Test Method for Static Modulus of Elasticity and Poisson's Ratio of Concrete in Compression. ASTM International.
Dabbaghi, F., Dehestani, M., Yousefpour, H., Rasekh, H., Navaratnam, S., 2021. Residual compressive stress–strain relationship of lightweight aggregate concrete after exposure to elevated temperatures. Construct. Build. Mater. 298, 123890.
Dawood, E.T., Alattar, A.A., Abbas, W.A., Mohammad, Y.Z., 2020. Behavior of foamed concrete reinforced with hybrid fibers and exposed to elevated temperatures. SN Appl. Sci. 2 (1), 84.
EN 1992-1-2, 2004. Eurocode 2: design of concrete structures – Part 1.2: general rules – structural fire design, 59. British Standard Institution, London, p. 20.
Galle, C., 2001. Effect of drying on cement-based materials pore structure as identified by mercury intrusion porosimetry: a comparative study between oven-, vacuum-, and freeze-drying. Cement Concr. Res. 31 (10), 1467–1477.
He, Z.H., Shen, M.L., Shi, J.Y., Yalçınkaya, Ç., Du, S.G., Yuan, Q., 2022. Recycling coral waste into eco-friendly UHPC: mechanical strength, microstructure, and environmental benefits. Sci. Total Environ. 836, 155424.
Hu, H., Wu, Y., Wei, Y., 2023. Recycling waste dolomite powder in cement paste: early hydration process, microscale characteristics, and life-cycle assessment. Sci. Total Environ. 902, 166008.
Jiang, D., Liu, Z., Christodoulatos, C., Conway, M., Bao, Y., Meng, W., 2022. Utilization of off-specification fly ash in preparing ultra-high-performance concrete (UHPC): mixture design, characterization, and life-cycle assessment. Resour. Conserv. Recycl. 180, 106136.
Li, V.C., 2003. On engineered cementitious composites (ECC) a review of the material and its applications. J. Adv. Concr. Technol. 1 (3), 215–230.
Li, Y., Pimienta, P., Pinoteau, N., Tan, K.H., 2019a. Effect of aggregate size and inclusion of polypropylene and steel fibers on explosive spalling and pore pressure in ultra-high-performance concrete (UHPC) at elevated temperature. Cement Concr. Compos. 99, 62–71.
Li, Y., Yang, E.H., Tan, K.H., 2019b. Effects of heating followed by water quenching on strength and microstructure of ultra-high performance concrete. Construct. Build. Mater. 207, 403–411.
Liang, X., Wu, C., Su, Y., Chen, Z., Li, Z., 2018. Development of ultra-high performance concrete with high fire resistance. Construct. Build. Mater. 179, 400–412.
Liu, J.C., Tan, K.H., 2018. Fire resistance of ultra-high performance strain hardening cementitious composite: residual mechanical properties and spalling resistance. Cement Concr. Compos. 89, 62–75.
Luo, B., Deng, C., Luo, Y., 2022. Mechanical properties and microstructure of UHPC with recycled glasses after exposure to elevated temperatures. J. Build. Eng. 62, 105369.
Magalhães, M.D.S., Toledo Filho, R.D., Fairbairn, E.D.M.R., 2015. Thermal stability of PVA fiber strain hardening cement-based composites. Construct. Build. Mater. 94, 437–447.
Olszak-Humienik, M., Jablonski, M., 2014. Thermal behavior of natural dolomite. J. Therm. Anal. Calorim. 119 (3), 2239–2248.
Phan, L.T., Carino, N.J., 2002. Effects of test conditions and mixture proportions on behavior of high-strength concrete exposed to high temperatures. ACI Mater. J. 99 (1), 54–66.
Ranade, R., Li, V.C., Stults, M.D., Heard, W.F., Rushing, T.S., 2013. Composite properties of high-strength, high-ductility concrete. ACI Mater. J. 110 (4).
Rawat, S., Lee, C.K., Zhang, Y.X., 2021. Performance of fibre-reinforced cementitious composites at elevated temperatures: a review. Construct. Build. Mater. 292, 123382.
Rawat, S., Zhang, Y.X., Lee, C.K., 2022. Multi-response optimization of hybrid fibre engineered cementitious composite using Grey-Taguchi method and utility concept. Construct. Build. Mater. 319, 126040.
Ren, G., Gao, X., Zhang, H., 2022. Utilization of hybrid sisal and steel fibers to improve elevated temperature resistance of ultra-high performance concrete. Cement Concr. Compos. 130, 104555.
Sahmaran, M., Lachemi, M., Li, V.C., 2010. Assessing mechanical properties and microstructure of fire-damaged engineered cementitious composites. ACI Mater. J. 107 (3), 297–304.
Shang, X., Lu, Z., 2014. Impact of high temperature on the compressive strength of ECC. Adv. Mater. Sci. Eng. 2014 https://doi.org/10.1155/2014/919078. Article ID 919078.
Shoji, D., He, Z., Zhang, D., Li, V.C., 2022. The greening of engineered cementitious composites (ECC): a review. Construct. Build. Mater. 327, 126701.
Sullivan, P.J.E., Sharshar, R., 1992. The performance of concrete at elevated temperatures (as measured by the reduction in compressive strength). Fire Technol. 28 (3), 240–250.
Taborda-Barraza, M., Pelisser, F., Gleize, P.J.P., 2021. Thermal-mechanical properties of metakaolin-based geopolymer containing silicon carbide microwhiskers. Cement Concr. Compos. 123, 104168.
Tang, J., Ma, W., Gu, Z., Zhang, Y., Fang, D., Zhao, L., 2023. Study on mechanical properties and microstructure of aluminate cement-based materials incorporating recycled brick powder after exposure to elevated temperatures. J. Build. Eng. 70, 106472.
Way, R.T., Wille, K., 2016. Effect of heat-induced chemical degradation on the residual mechanical properties of ultrahigh-performance fiber-reinforced concrete. J. Mater. Civ. Eng. 28 (4), 1–10.
Wu, J.-D., Guo, L.-P., Qin, Y.-Y., 2021. Preparation and characterization of ultra-high-strength and ultra-high-ductility cementitious composites incorporating waste clay brick powder. J. Clean. Prod. 312, 127813.
Xuan, M.Y., Bae, S.C., Kwon, S.J., Wang, X.Y., 2022. Sustainability enhancement of calcined clay and limestone powder hybrid ultra-high-performance concrete using belite-rich Portland cement. Construct. Build. Mater. 351, 128932.
Yu, K.Q., Dai, J.G., Lu, Z.D., Leung, C.K.Y., 2015. Mechanical properties of engineered cementitious composites subjected to elevated temperatures. J. Mater. Civ. Eng. 27 (10), 04014268.
Zhang, Z., Liu, S., Yang, F., Weng, Y., Qian, S., 2021a. Sustainable high strength, high ductility engineered cementitious composites (ECC) with substitution of cement by rice husk ash. J. Clean. Prod. 317, 128379.
Yu, J., Weng, W., Yu, K., 2014. Effect of different cooling regimes on the mechanical properties of cementitious composites subjected to high temperatures. Sci. World J. 2014 https://doi.org/10.1155/2014/289213. Hindawi.
Zhang, D., Liu, Y., Tan, K.H., 2021b. Spalling resistance and mechanical properties of strain-hardening ultra-high performance concrete at elevated temperature. Construct. Build. Mater. 266, 120961.
Zhang, X., Wu, Z., Xie, J., Hu, X., Shi, C., 2024. Trends toward lower-carbon ultra-high performance concrete (UHPC)–A review. Construct. Build. Mater. 420, 135602.
Zhong, H., Zhang, M., 2021. Effect of recycled tyre polymer fibre on engineering properties of sustainable strain hardening geopolymer composites. Cement Concr. Compos. 122, 104167.